J. Fluid Mech. (1988), *vol.* 193, *pp.* 445–473
Printed in Great Britain

Reheat buzz: an acoustically coupled combustion instability. Part 2. Theory

By G. J. BLOXSIDGE†, A. P. DOWLING‡ AND P. J. LANGHORNE‖

† British Maritime Technology, CEEMAID Division, St Johns Street, Hythe, Southampton SO4 6YS, UK

‡ The University Engineering Department, Trumpington Street, Cambridge CB2 1PZ, UK

‖ Department of Physics, University of Otago, PO Box 56, Dunedin, New Zealand

(Received 21 August 1987)

Reheat buzz is a low-frequency instability of afterburners. It is caused by the interaction of longitudinal acoustic waves and unsteady combustion. Similar combustion instabilities occur in laboratory rigs. A theory is developed to determine the frequency and mode shape of the instability and is tested by comparison with the experimental results described in Part 1. The predicted and measured frequencies are found to be within 6 Hz (7%) of each other. The theory is able to predict the observed variation of frequency with equivalence ratio, inlet Mach number and geometry.

1. Introduction

Reheat buzz is a low-frequency combustion instability of afterburners. Langhorne (1988) (hereinafter referred to as Part 1) has investigated a similar instability on a laboratory rig in which a premixed flame burns in a duct. The ultimate aim of our theoretical work is to develop a prediction scheme for afterburners, so that the frequency of the buzz mode and onset fuel–air ratio may be predicted at the design stage. As an initial step, the theory has been developed and tested by comparison with experimental results for the rig.

Since the frequencies of the buzz mode are low and their wavelengths long in comparison with the duct diameter, only plane acoustic waves carry energy. We therefore just consider one-dimensional disturbances. Previous work (Dowling & Bloxsidge 1984) has considered the burning zone to be short in comparison with the wavelength. However, the experiments on the rig described in Part 1 show that burning persists throughout the region downstream of the flame-holder, a length which can be an appreciable fraction of the wavelength. We therefore include distributed heat release. The description of the propagation of acoustic waves in regions of varying temperature is straightforward (see for example Barton 1986). Similarly, the way in which unsteady combustion generates sound is well established (Cumpsty 1979). The main difficulty in an investigation of thermo-acoustic oscillations is in describing the influence of the unsteady flow on the rate of combustion. Rayleigh's criterion indicates how important this interaction is, for as well as altering the frequency (Rayleigh 1896), the phase relationship between the unsteady pressure and heat release will determine whether acoustic modes are damped or augmented by the unsteady combustion.

Marble & Candel (1978) investigate theoretically the response of a flame anchored

in a duct to oncoming linear perturbations. That work has been extended by Subbaiah (1983) and to compressible flows by Le Chatelier & Candel (1981). However, in all cases, it is assumed that the burning occurs in a thin front with a uniform and constant flame speed. The flame spreads smoothly from the centre-body and combustion is complete when it meets the duct walls. Therefore this work probably has little relevance to our rig in which the axial extent of the combustion zone is much longer. Moreover, the flame speed has been observed to vary appreciably during one cycle in a similar experiment by Campbell, Bray & Moss (1983).

Since the flow involves additional coherent acoustic perturbations to a turbulent flow, rather than attempt an analytical solution for the relationship between flow unsteadiness and the instantaneous rate of heat release, we seek an empirical model. Bray *et al.* (1983) also used an empirical closure for their equations of motion. They assumed that the pressure perturbation just upstream of the flame-holder lagged the downstream pressure by $\frac{1}{2}\pi$. However, their subsequent experiments showed that this criterion was not generally met. We seek a fundamental flame model: one that describes how the rate of heat release is influenced by flow perturbations near the flame-holder. Such models are well developed for gas and oil burner ports (see for example Merk 1956; Hadvig 1971; Mugridge 1980). Our aim is for a similar understanding of the afterburner geometry.

The analysis is essentially a one-dimensional stability theory for acoustic waves in a duct. A general disturbance can be Fourier transformed into modes each with time dependence $e^{i\omega t}$. Linear perturbations are considered and so each mode may be investigated separately. The equations of motion are developed for linear disturbances in a duct with heat release and a mean flow. These equations can be readily solved once the heat release rate is specified. It is found that only disturbances with certain discrete values of ω can exist as free modes of the flame/duct arrangement. If the imaginary part of ω is negative the disturbance grows in time and the system is unstable. Real ω gives the frequency of this unstable mode.

In §2 we assume the rate of heat release to be proportional to the measured light emission from C_2 radicals, and calculate the predicted mode shapes and buzz frequency. The calculated results are in excellent agreement with the measurements. This provides a reassuring check on the various assumptions made. It is evidently sufficient to consider only one-dimensional flow. We also have confirmation that, for our purposes at least, it is adequate to take the heat release rate to be directly proportional to the light emission. However, since such calculations require the measured unsteady heat release as an input, they hardly constitute a prediction of buzz!

Section 3 deals with the development of a heat release model. The rig is run at a low fuel–air ratio at which the flame is stable with no discernible narrow-band buzz peak in the pressure spectrum. Then acoustic waves are generated in the rig by a movable centre-body, and the response of the flame investigated. We use these measurements to determine how the instantaneous rate of heat release is related to perturbations at the flame-holder. The flame must respond to changes in particle velocity, pressure and temperature near the flame-holder. But the Mach number of the mean flow is low and so the fractional change in velocity is much larger than the fractional change in pressure and temperature near the flame-holder. This was evident in the experimental results described in Part 1 where the flame was observed to move intermittently upstream of the flame-holder (indicating velocity per-

turbations of the order of the mean velocity), while fractional changes in pressure were less than 10%. Since the fractional changes in velocity are so much larger than the other fractional changes in the flow, it is reasonable to assume the unsteady rate of combustion to be principally determined by velocity fluctuations near the flameholder. This supposition is confirmed by the data collapsing into a universal form when expressed in this way. Poinsot *et al.* (1986) excited a flame in a duct in a similar experiment. They used their results to determine a reflection coefficient. But as they point out, this reflection coefficient depends not only on the flame but also on the downstream geometry. In determining the relationship between fluctuations in heat release rate and particle velocity we have determined a more general flame model which can be applied to different geometries and mean flows.

The wider applicability of our flame model is demonstrated in §4 where the same model is used to predict mode shapes and buzz frequencies for the rig for different fuel–air ratios, mean velocities and lengths upstream or downstream of the flameholder. In all cases the measured and calculated frequencies are in good agreement with each other. The maximum error being 6 Hz (7%). Further confirmation of the theory is obtained by a comparison of the measured and calculated modal pressure distributions. The theory is accurately able to predict the unsteady pressure changes throughout the combustion region.

2. Linear stability analysis of a flame in a duct

The geometry of the experimental rig has been described in Part 1 and is illustrated in figure 1. The working section is a duct of circular cross-section, whose length L can be varied. Premixed fuel and air enter the working section through a choked nozzle, and burn in the wake of a bluff body consisting of a conical gutter supported on a stem. We choose a coordinate system in which the origin, $x = 0$, is at the choked inlet of the working section and x increases towards the hot duct exit. Since the theory is linear, it is sufficient just to investigate perturbations to the mean flow with time dependence $e^{i\omega t}$. A computer program has been written to calculate the complex eigenfrequencies, ω, for which the boundary conditions at both ends of the duct are satisfied. The sign of the imaginary part of ω determines the stability, while $\mathrm{Re}\,\omega$ gives the frequency of the mode. The frequencies of interest are low, with wavelengths long in comparison with the duct diameter. As only plane acoustic waves carry energy, we consider the flow to be one-dimensional.

Mean values will be denoted by an overbar so that the axial velocity $u(x,t)$, for example, can be expressed as

$$u(x,t) = \bar{u}(x) + u'(x,t),$$

where the fluctuating component $u'(x,t) = \mathrm{Re}\,(\hat{u}(x)\,e^{i\omega t})$. The pressure p, density ρ and temperature T may be expanded in a similar way. When investigating the development of the flow along a duct of cross-sectional area $A(x)$, it is convenient to introduce m, F and E, respectively the mass, momentum and energy flow rates. They are defined by

$$m = \rho u A, \quad F = (p + \rho u^2)\,A, \quad E = m(c_p T + \tfrac{1}{2}u^2), \tag{2.1}$$

with c_p the specific heat capacity at constant pressure.

In sections of the duct with uniform cross-sectional area, the mean values of the equations of mass, momentum and energy conservation give

$$\frac{d\bar{m}}{dx} = 0, \quad \frac{d\bar{F}}{dx} = 0, \quad \frac{d\bar{E}}{dx} = \bar{q}(x), \tag{2.2}$$

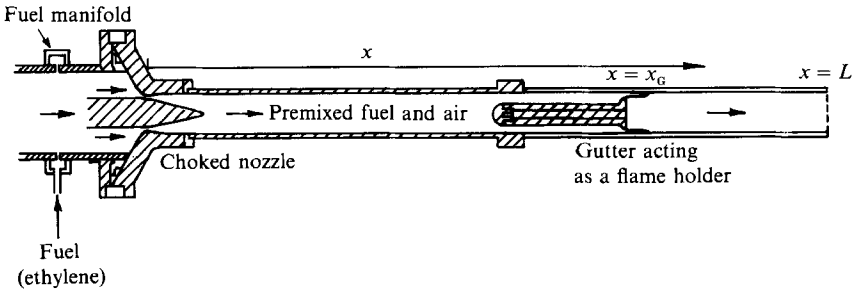

FIGURE 1. The geometry of the rig.

where $q(x,t) = \bar{q}(x) + q'(x,t)$ is the instantaneous heat release rate per unit length of ducting. When $\bar{q}(x)$ is specified, (2.2) may be readily integrated with respect to x, to determine any development of the mean mass, momentum and energy flows throughout portions of the duct of uniform cross-sectional area. After some algebraic manipulation the other mean flow parameters can be expressed in terms of $\bar{m}$, $\bar{F}$ and $\bar{E}$ by combining the equation of state for a perfect gas,

$$\bar{p} = R\bar{\rho}\bar{T}, \tag{2.3}$$

with the definitions in (2.1). In detail these relationships are

$$\bar{u} = \frac{\gamma\bar{F}}{(\gamma+1)\,\bar{m}}\left[1-\left(1-\frac{2(\gamma^2-1)\,\bar{m}\bar{E}}{\gamma^2\bar{F}^2}\right)^{\frac{1}{2}}\right], \tag{2.4a}$$

$$\bar{p} = (\bar{F}-\bar{m}\bar{u})/A, \quad \bar{\rho} = \bar{m}/A\bar{u}, \quad \bar{T} = \bar{p}/R\bar{\rho}, \tag{2.4b,c,d}$$

where γ is the ratio of specific heat capacities.

At the upstream end of the stem supporting the gutter and, more importantly, at the gutter itself, the duct area available to the flow abruptly decreases and a force is exerted on the fluid. The change in the mean flow across these contractions is determined from the conservation of mass and energy flow rates and the fact that the flow is isentropic. These conditions give

$$\bar{m}_2 = \bar{m}_1, \quad \bar{E}_2 = \bar{E}_1, \quad \bar{p}_2/\bar{\rho}_2^{\gamma} = \bar{p}_1/\bar{\rho}_1^{\gamma}. \tag{2.5}$$

The suffices 1 and 2 denote the flow just upstream and downstream of the area change. It is a matter of straightforward algebra to use (2.1), (2.3) and (2.5) to solve for the flow downstream of a contraction in terms of the upstream flow.

It is not reasonable to assume the flow to be one-dimensional in the wake of the gutter. Instead this region is enclosed by a control volume as shown in figure 2. The volume is to be sufficiently long that one-dimensional flow is re-established by its downstream end. Conservation of mass, momentum and energy are applied across the control volume, together with a Kutta condition that pressure is uniform over its upstream surface. This shows the downstream flow to be related to the flow at the gutter lip by

$$\bar{m}_D = \bar{m}_G, \quad \bar{F}_D = \bar{F}_G + \bar{p}_G(A_D - A_G) \quad \bar{E}_D = \bar{E}_G + \bar{Q}_C, \tag{2.6a,b,c}$$

where conditions at the gutter lip are denoted by the suffix G, and D indicates the downstream end of the control volume. $\bar{Q}_C$ is the mean rate of heat release within the volume;

$$\bar{Q}_C = \int_{x_G}^{x_D} \bar{q}(x)\,dx. \tag{2.7}$$

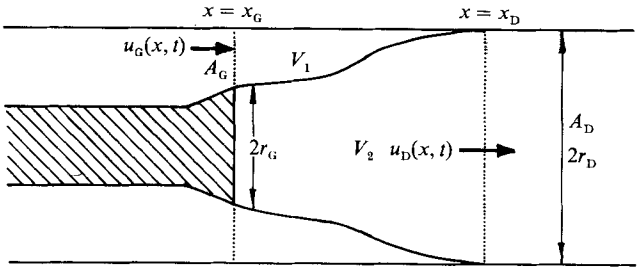

FIGURE 2. Control volume enclosing the region just downstream of the gutter.

Equation (2.6) shows that the mean flow at exit from the control volume may be readily calculated from the conditions at inlet.

If the mean flow were known at one axial position, (2.2) could be integrated with respect to x and, together with the jump conditions expressed in (2.5) and (2.6), would determine the flow further downstream. However, the mean flow satisfies mixed point boundary conditions. The inlet Mach number and temperature are known and the exit pressure is atmospheric. The scheme adopted is to guess the upstream pressure, integrate down the duct and then iterate in the value of the guess for the mean upstream pressure until the mean exit pressure is atmospheric.

Having developed a scheme for calculating the mean flow, we now turn our attention to the unsteady flow. Again it is convenient to work with mass, momentum and energy flow rates. We denote their fluctuations by m', F' and E' respectively. For linear disturbances

$$m' = (\rho'\bar{u} + \bar{\rho}u')\,A, \tag{2.8a}$$

$$F' = (p' + \rho'\bar{u}^2 + 2\bar{\rho}\bar{u}u')\,A, \tag{2.8b}$$

$$E' = m'(c_p\bar{T} + \tfrac{1}{2}\bar{u}^2) + \bar{m}(c_pT' + \bar{u}u'), \tag{2.8c}$$

and the equation of state reduces to

$$\frac{p'}{\bar{p}} = \frac{\rho'}{\bar{\rho}} + \frac{T'}{\bar{T}}. \tag{2.9}$$

The perturbations in axial velocity, pressure and temperature may be expressed explicitly in terms of m', F' and E' and the mean flow. After some algebraic manipulation the perfect gas law (2.9), together with (2.8), may be used to show that

$$u' = \frac{\frac{1}{2}(\gamma+1)\,\bar{u}^2m' - \gamma\bar{u}F' + (\gamma-1)\,E'}{(\gamma\bar{p} - \bar{\rho}\bar{u}^2)\,A}, \tag{2.10a}$$

with

$$\rho' = \frac{m'}{\bar{u}A} - \frac{\bar{\rho}u'}{\bar{u}}, \quad p' = \frac{F'}{A} - \bar{\rho}\bar{u}u' - \frac{\bar{u}m'}{A}, \tag{2.10b,c}$$

and

$$T' = \frac{E'}{c_p\bar{m}} - \frac{m'}{\bar{m}}\left(\bar{T} + \frac{\bar{u}^2}{2c_p}\right) - \frac{\bar{u}u'}{c_p}. \tag{2.10d}$$

For linear disturbances proportional to $e^{i\omega t}$, the equations of mass, momentum and energy conservation in a duct of uniform cross-sectional area A are

$$\frac{d\hat{m}}{dx} = -i\omega A\hat{\rho}, \quad \frac{d\hat{F}}{dx} = -i\omega\hat{m}, \tag{2.11a,b}$$

and
$$\frac{\mathrm{d}\hat{E}}{\mathrm{d}x} = \hat{q} - \mathrm{i}\omega A(\hat{\rho}(c_v \bar{T} + \tfrac{1}{2}\bar{u}^2) + \bar{\rho}(c_v \hat{T} + \bar{u}\hat{u})). \tag{2.11c}$$

As before, the circumflex denotes the complex amplitude of the disturbances of frequency ω. Linearization requires the pressure perturbation to be very much less than the mean pressure, and the fluctuations in velocity to be a small fraction of the sound speed. The velocity variation may, however, be an appreciable proportion of the mean velocity.

When the mean flow, the frequency ω and the relationship between $q'(x,t)$ and the flow are specified and the flow perturbations are given at one axial position, (2.11) can be integrated numerically with respect to x. Then, together with the algebraic relationships described by (2.10), it determines the flow perturbations at positions downstream.

Again, across abrupt contractions in duct area, we use conservation of mass and energy and the fact that the flow through the contraction is isentropic to relate the downstream flow (denoted by the suffix 2) to that just upstream of the area change (suffix 1). Provided the contraction occurs over a length short in comparison with the wavelength
$$\hat{m}_2 = \hat{m}_1, \quad \hat{E}_2 = \hat{E}_1, \quad \frac{\hat{p}_2}{\bar{p}_2} - \frac{\gamma\hat{\rho}_2}{\bar{\rho}_2} = \frac{\hat{p}_1}{\bar{p}_1} - \frac{\gamma\hat{\rho}_1}{\bar{\rho}_1}. \tag{2.12}$$

A combination of (2.10), (2.11) and (2.12) enables the downstream flow to be calculated in terms of the upstream flow.

Care must be taken when applying conservation relationships to the control volume enclosing the wake of the gutter. Schlieren photographs show moving interfaces with strong density gradients in this region. These interfaces indicate the existence of a flame front at which combustion is initiated. There is a significant drop in mean density across this flame front. As the flame front moves in response to the flow disturbances, the proportion of hot to cold gas within the control volume changes. This alters the mass, momentum and energy stored within the volume, an effect which must be included in the conservation equations.

We will denote the volume of the unburnt gas within the control volume by V_1, while V_2 is the volume occupied by the hot gas within this control volume (see figure 2). Conservation of mass applied to the volume $V_1 + V_2$ shows that
$$m_G - m_D = \frac{\mathrm{d}}{\mathrm{d}t}\int_{V_1+V_2} \rho \,\mathrm{d}V, \tag{2.13}$$

where once again m is the mass flow rate and conditions at the gutter lip and at the downstream end of the control volume are denoted by the suffices G and D respectively. Assuming that the flow in V_1 may be approximated by that at the gutter lip and the flow within V_2 by that at $x = x_D$, we have
$$m_G - m_D = \frac{\mathrm{d}}{\mathrm{d}t}(\rho_G V_1) + \frac{\mathrm{d}}{\mathrm{d}t}(\rho_D V_2), \tag{2.14}$$

Equation (2.6a) may be recovered from the mean value of (2.14), while for linear perturbations of frequency ω it gives
$$\hat{m}_G - \hat{m}_D = (\bar{\rho}_G - \bar{\rho}_D)\frac{\mathrm{d}\widehat{V_1}}{\mathrm{d}t} + \mathrm{i}\omega(\hat{\rho}_G \bar{V}_1 + \hat{\rho}_D \bar{V}_2), \tag{2.15}$$

since the sum of the volumes, V_1+V_2, is constant. Similar arguments lead to the linearized momentum and energy equations for the control volume:

$$\hat{F}_G-\hat{F}_D+\hat{p}_G(A_D-A_G)=(\bar{\rho}_G\bar{u}_G-\bar{\rho}_D\bar{u}_D)\frac{\widehat{dV_1}}{dt}$$
$$+i\omega((\hat{\rho}_G\bar{u}_G+\bar{\rho}_G\hat{u}_G)\bar{V}_1+(\hat{\rho}_D\bar{u}_D+\bar{\rho}_D\hat{u}_D)\bar{V}_2), \quad (2.16)$$

and

$$\hat{E}_G-\hat{E}_D+\hat{Q}_C=(\hat{\rho}_G(c_V\bar{T}_G+\tfrac{1}{2}\bar{u}_G^2)-\bar{\rho}_D(c_V\bar{T}_D+\tfrac{1}{2}\bar{u}_D^2))\frac{\widehat{dV_1}}{dt}$$
$$+i\omega(\hat{\rho}_G(c_V\bar{T}_G+\tfrac{1}{2}\bar{u}_G^2)\bar{V}_1+\bar{\rho}_G(c_V\bar{T}_G+\bar{u}_G\hat{u}_G)\bar{V}_1$$
$$+\hat{\rho}_D(c_V\bar{T}_D+\tfrac{1}{2}\bar{u}_D^2)\bar{V}_2+\bar{\rho}_D(c_V\hat{T}_D+\bar{u}_D\hat{u}_D)\bar{V}_2). \quad (2.17)$$

A new unsteady variable $\widehat{dV_1}/dt$ has been introduced in the right-hand side of (2.15)–(2.17). But consideration of mass conservation in V_1 will show that this can be related to the rate of heat release at the flame front. For the volume V_1 we have

$$m_G-m_F=\frac{d}{dt}\int_{V_1}\rho\,dV, \quad (2.18)$$

where m_F is the mass flow rate through the flame front separating V_1 and V_2. The mean of (2.18) is

$$\bar{m}_G-\bar{m}_F=0. \quad (2.19a)$$

With the density in V_1 approximated by that at the gutter lip, (2.18) gives

$$\hat{m}_G-\hat{m}_F=\rho_G\frac{\widehat{dV_1}}{dt}+i\omega\hat{\rho}_G\bar{V}_1, \quad (2.19b)$$

for linear perturbations. The mass flow rate through the flame front, m_F, is directly proportional to the rate of heat release at the flame front, Q_C, for a premixed gas with uniform fuel–air ratio. This fact, together with (2.19a), can be used to show that $\hat{m}_F=\bar{m}_G\hat{Q}_C/\bar{Q}_C$. Substitution for $\hat{m}_F$ in (2.19b) then leads to

$$\frac{\widehat{dV_1}}{dt}=\frac{\hat{m}_G}{\bar{\rho}_G}-\frac{\bar{m}_G\hat{Q}_C}{\bar{\rho}_G\bar{Q}_C}-\frac{i\omega\hat{\rho}_G\bar{V}_1}{\bar{\rho}_G}, \quad (2.20)$$

enabling the volume derivatives $\widehat{dV_1}/dt$ appearing on the right-hand side of (2.15)–(2.17) to be replaced by other flow variables.

The mean values of the volumes V_1 and V_2 also occur in terms on the right-hand side of (2.15)–(2.17). These terms are small if the control volume is short in comparison with the wavelength, but will be retained for completeness. However, since they only represent small corrections, we can be crude in the way we estimate $\bar{V}_1$ and $\bar{V}_2$. Assuming that on average the flame sheet takes the shape of the surface of a truncated cone of axial length x_D-x_G, straightforward geometry may be used to calculate the volumes $\bar{V}_1$ and $\bar{V}_2$. Suppose the duct has internal radius r_D and the gutter lip is of radius r_G. Then

$$\bar{V}_1=\tfrac{1}{3}\pi(x_D-x_G)(2r_D^2-r_Dr_G-r_G^2), \quad \bar{V}_2=\tfrac{1}{3}\pi(x_D-x_G)(r_D^2+r_Dr_G+r_G^2). \quad (2.21)$$

When the expressions for $\widehat{dV_1}/dt$, $\bar{V}_1$ and $\bar{V}_2$ from (2.20) and (2.21) are substituted into (2.15)–(2.17), the unsteady flow at the downstream end of the control volume

can be expressed in terms of the mean flow and the unsteady flow at inlet, provided the unsteady heat release rate $\hat{Q}_C$ is known. It is therefore possible to calculate the downstream flow, once the flow at the gutter lip has been determined.

The nozzle at the upstream end of the duct is choked. This means that acoustic perturbations within the working section will not alter the mass flow rate at inlet which therefore remains constant and we have

$$\frac{\hat{\rho}(0)}{\bar{\rho}(0)}+\frac{\hat{u}(0)}{\bar{u}(0)}=0. \tag{2.22}$$

Moreover, care was taken to ensure that the flow was only just choked, so that any shocks are weak and there is negligible entropy production. The flow is therefore isentropic, with

$$\frac{\hat{p}(0)}{\bar{p}(0)}=\frac{\gamma\hat{\rho}(0)}{\bar{\rho}(0)}. \tag{2.23}$$

Since the theory is linear, if $\hat{p}(x)\,\mathrm{e}^{\mathrm{i}\omega t}$ satisfies the homogeneous equations of motion, so will $\alpha\hat{p}(x)\,\mathrm{e}^{\mathrm{i}\omega t}$, for any complex constant α. Consequently we may choose without loss of generality, that

$$\hat{p}(0)=1. \tag{2.24}$$

When (2.22)–(2.24) are combined with the perfect gas equation they completely specify the unsteady inlet flow.

With the flow at $x=0$ determined, the unsteady flow throughout the duct may be calculated provided the relationship between $q'(x,t)$ and the flow is known. For a given frequency ω, integration of (2.11) with respect to x, together with the jump conditions expressed in equations (2.12), (2.15)–(2.17) and (2.20)–(2.21) determines the flow perturbations further downstream. The downstream end of the working section is open and we apply Howe's (1979) boundary condition there:

$$(1+\bar{M})\left(1-\bar{M}-\frac{1}{4}\left(\frac{\omega r_D}{\bar{c}}\right)^2-0.6133\mathrm{i}\left(\frac{\omega r_D}{\bar{c}}\right)\right)(\hat{p}+\bar{\rho}\bar{c}\hat{u})$$

$$+(1-\bar{M})\left(1+\bar{M}+\frac{1}{4}\left(\frac{\omega r_D}{\bar{c}}\right)^2+0.6133\mathrm{i}\left(\frac{\omega r_D}{\bar{c}}\right)\right)(\hat{p}-\bar{\rho}\bar{c}\hat{u})=0 \quad \text{at } x=L, \tag{2.25}$$

$\bar{M}=\bar{u}/\bar{c}$ is the mean Mach number. The boundary condition (2.25) includes end corrections due to finite mean velocity and duct diameter but, for the values of these parameters in our rig, differs little from $\hat{p}(L)=0$. For a general value of ω, the exit boundary condition (2.25) is not satisfied. We therefore iterate in ω, at each step calculating the flow in the duct, until we determine the complex value of ω for which the expression in (2.25) vanishes. Only disturbances with these particular frequencies satisfy all the boundary conditions and can exist as free modes of the duct/flame arrangement. The mode shape has also been determined.

The theory described enables us to calculate the unsteady flow through a premixed flame anchored in a duct. If suitable boundary conditions are applied at the ends of the duct, the onset and frequency of longitudinal combustion oscillations can be predicted. However, the theory depends crucially upon a form for the mean and unsteady heat release which must be specified in order to complete the calculations. As a first step we will use the light emission data presented in Part 1 to describe these important functions.

Denote the light emission from C_2 radicals per unit length of ducting by

Configuration 1	Configuration 2	Configuration 3	Configuration 4
$x_G = 1.18$ m	$x_G = 0.74$ m	$x_G = 1.19$ m	$x_G = 1.18$ m
$L = 1.92$ m	$L = 1.48$ m	$L = 2.18$ m	$L = 1.92$ m
$\bar{M}_u = 0.08$	$\bar{M}_u = 0.08$	$\bar{M}_u = 0.08$	$\bar{M}_u = 0.15$
$x_{ref} = 0.75$ m	$x_{ref} = 0.49$ m	$x_{ref} = 0.76$ m	$x_{ref} = 0.75$ m

$\bar{M}_u$ denotes the Mach number upstream of the combustion zone. The inlet static temperature, $\bar{T}_u$, is 288 K, the duct radius, r_D, 35 mm and the gutter radius, r_G, 17 mm for all configurations.

TABLE 1

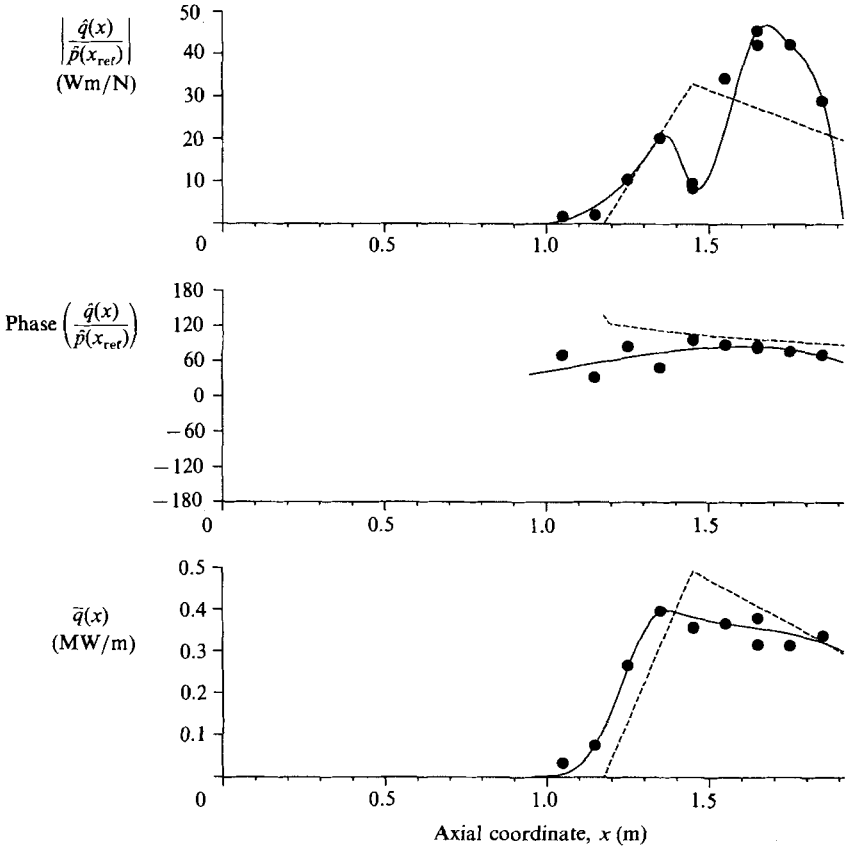

FIGURE 3. The mean and unsteady heat release rates/unit length at the buzz frequency for configuration 1, $\phi = 0.70$. ●, experimental points; ——, spline fit; – – –, established flame model.

$i(x,t) = \bar{i}(x) + i'(x,t)$. We speculate that the heat release rate is directly proportional to this light emission and write

$$q(x,t) = ki(x,t). \tag{2.26}$$

Equation (2.26) may be readily decomposed into its mean and fluctuating components, which we choose to write as

$$\bar{q}(x) = k\bar{i}(x), \tag{2.27}$$

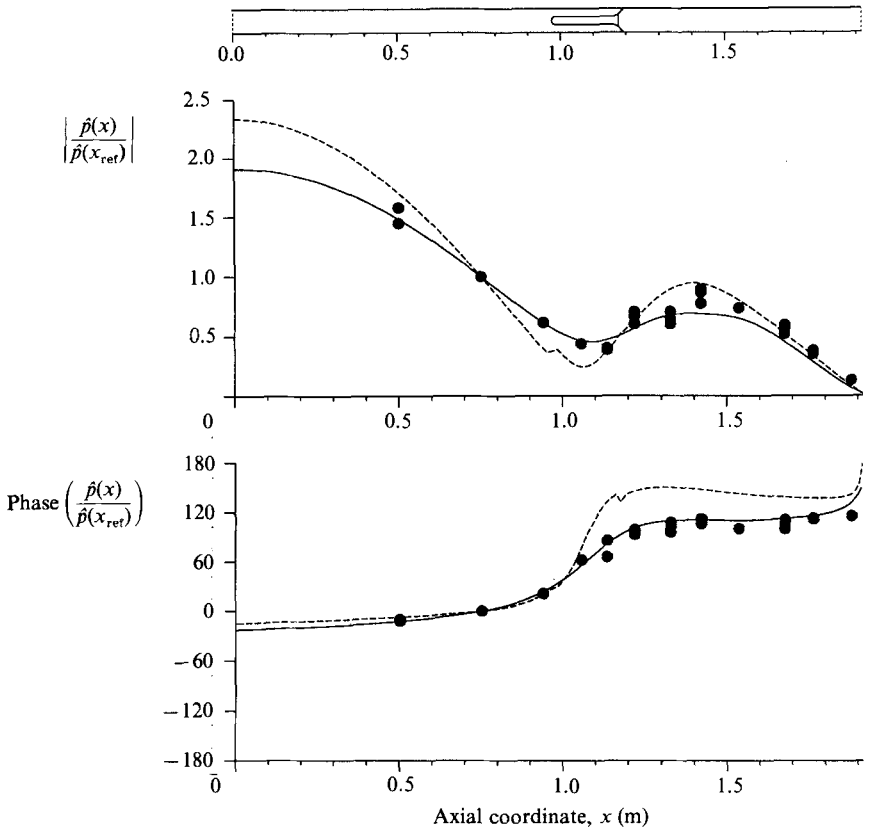

FIGURE 4. The pressure variation along the duct at the buzz frequency for configuration 1, $\phi = 0.70$. ●, experimental points; ——, calculated using the spline fit to the heat release data; – – –, calculated using the established flame model.

and
$$\frac{\hat{q}(x)}{\hat{p}(x_{\text{ref}})} = k\frac{\hat{\imath}(x)}{\hat{p}(x_{\text{ref}})}, \tag{2.28}$$

since the measured transfer functions were referenced with respect to the pressure at x_{ref}.

Integration of (2.27) along the duct indicates how the constant k can be determined:
$$k = \int_0^L \bar{q}(x)\,\mathrm{d}x \Big/ \int_0^L \bar{\imath}(x)\,\mathrm{d}x. \tag{2.29}$$

The integral of $\bar{\imath}(x)$ may be calculated directly from the light emission data. The integral of $\bar{q}(x)$ is the total mean heat release rate within the duct. It is equal to $c_{\text{p}}\bar{m}\Delta T_0$, where ΔT_0, the stagnation temperature rise along the duct, can be measured in a straightforward way. The mean light emission data, for the geometry and flow conditions of configuration 1 listed in table 1 and an equivalence ratio of 0.70, were described in Part 1. These, together with measurements of stagnation temperature, give k to be 7.3 kW/V.

Once k has been determined, the measured light emission data can be scaled by k to give predictions for the mean and fluctuating heat release rates per unit length. These are plotted in figure 3. Least-square cubic-splines were fitted to these local

estimates of $\bar{q}(x)$ and $\hat{q}(x)/\hat{p}(x_{\mathrm{ref}})$ to give a form for the distribution of heat release rate along the duct. The spline fits to the data are also shown in figure 3.

This empirical flame model may be used to calculate the perturbation to the flow. For simplicity the effect of gutter blockage will be neglected. An iteration for the frequency of oscillation yields a solution of 76.4 Hz compared with the measured value of 77 Hz. The calculated growth rate, $-\mathrm{Im}\,\omega$, is $+47.3\ \mathrm{s}^{-1}$, indicating the flame to be unstable at these conditions. The calculated modal pressure distribution is compared with the measured values in figure 4. The experimental pressures are normalized so that the experimental and calculated pressure perturbation coincide at x_{ref}, a step justified by the linearity of the problem. The calculated mode shape of the unsteady pressure fluctuations lies within the experimental error of the measured points. Very crudely, the mode shape of the pressure distribution is a quarter wave, with a maximum at the upstream end and a node near the gutter. A comparison of figures 3 and 4 shows that the heat release rate per unit length is approximately in phase with the unsteady pressure along a significant proportion of the length of the flame. Consequently, by Rayleigh's criterion, there is strong driving towards instability as indicated by the large value of the calculated growth rate.

The excellent agreement between the measured and calculated frequency of the oscillation and its mode shape is encouraging. It provides a reassuring check on the various assumptions made. It is evidently sufficient to consider only one-dimensional flow. We also have confirmation that, for our purposes at least, it is adequate to take the heat release rate to be directly proportional to the light emission. Moreover, the boundary conditions are validated. However, since the calculations require the measured unsteady heat release as an input, they hardly constitute a prediction scheme. In the next section we describe an experiment to determine a universally applicable model for the heat release rate.

3. Development of the flame model

We have seen that, once the heat release rate is specified as a function of axial position x, the theory described in §2 may be used to calculate the frequency and mode shape of the combustion oscillation. In this section an empirical flame model for the heat release rate will be developed from the results of a set of experiments on our laboratory flame.

The method adopted is to run the rig at a low fuel–air ratio for which the flame is stable and there is no discernible narrow-band peak in the light or pressure spectra. Then acoustic waves are artificially generated in the rig at a number of discrete frequencies. By studying the response of the flame to these perturbations in the flow it is possible to build an empirical flame model that can be applied to other geometries and flow conditions.

In order to perturb the flame, the fixed nozzle at inlet to the working section was replaced by a nozzle with a movable centre-body, which is mechanically coupled to a commercial vibrator as shown in figure 5. The arrangement is described in detail in Bloxsidge *et al.* (1988). Axial motion of the shaped centre-body alters the blockage to the oncoming gas, thereby producing a fluctuating mass flow into the working section and generating acoustic waves. The geometry and mean flow of configuration 1 in table 1 were used in these experiments and the equivalence ratio was maintained at 0.57. The vibrator was excited by sinusoidal signals of various amplitudes with frequencies in the range 15–95 Hz. The unsteady pressure and $I(x,t)$, the light emission from C_2 radicals in 0.1 m lengths of duct centred on x, were recorded. The

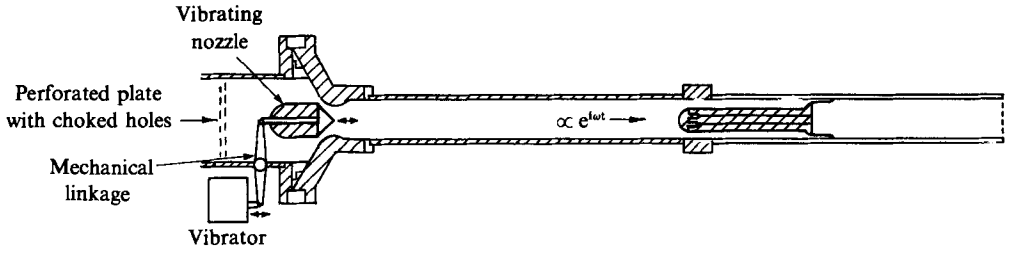

FIGURE 5. The geometry used to perturb the flame at different discrete frequencies.

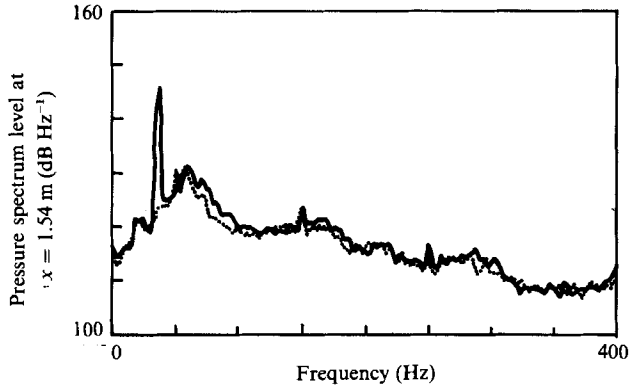

FIGURE 6. The pressure spectra at $x = 1.54$ m with and without forcing at 35 Hz. The amplitude of the forced centre-body movement is 2.4 mm peak-to-peak.

moving centre-body was found to be an effective acoustic source. Figure 6 shows a comparison between pressure spectra obtained when the centre-body was vibrated at 35 Hz and when it was fixed. It can be seen that the narrow-band peak in the forced oscillation is significantly higher than the level without forcing. Similar narrow-band peaks occur in the light emission data. At the frequency of the forcing all the unsteady measurements have coherences of 0.95 or better (typically 0.99 in the case of pressure measurements), indicating a signal-to-noise of at least ten to one. Reliable transfer functions can therefore be determined.

The theory has been developed for a linear unsteady flow. The induced oscillations should, therefore, be sufficiently weak that the measured transfer functions are independent of amplitude. To check this, the flow was driven at three levels of centre-body movement: 1.7, 2.4 and 3.1 mm peak-to-peak. Most of the experimental measurements were performed at the 2.4 mm level, while random checks were done by duplicating measurements at 1.7 mm and 3.1 mm levels. At the lower level, 1.7 mm, the coherences were only just acceptable, while at the highest level, 3.1 mm, the amplifier for the vibrator was drawing maximum permitted current for the highest frequency case, 95 Hz. These linearity checks are shown for the data displayed in figures 7, 8 and 10. In general the transfer functions were found to be reasonably constant.

The results for the light emission obtained by forcing at 45 Hz are displayed in figure 7. In all, transfer functions were measured at nine different frequencies but similar trends were observed. At this low equivalence ratio the mean light output per unit length is found to increase linearly with distance downstream of the gutter (see

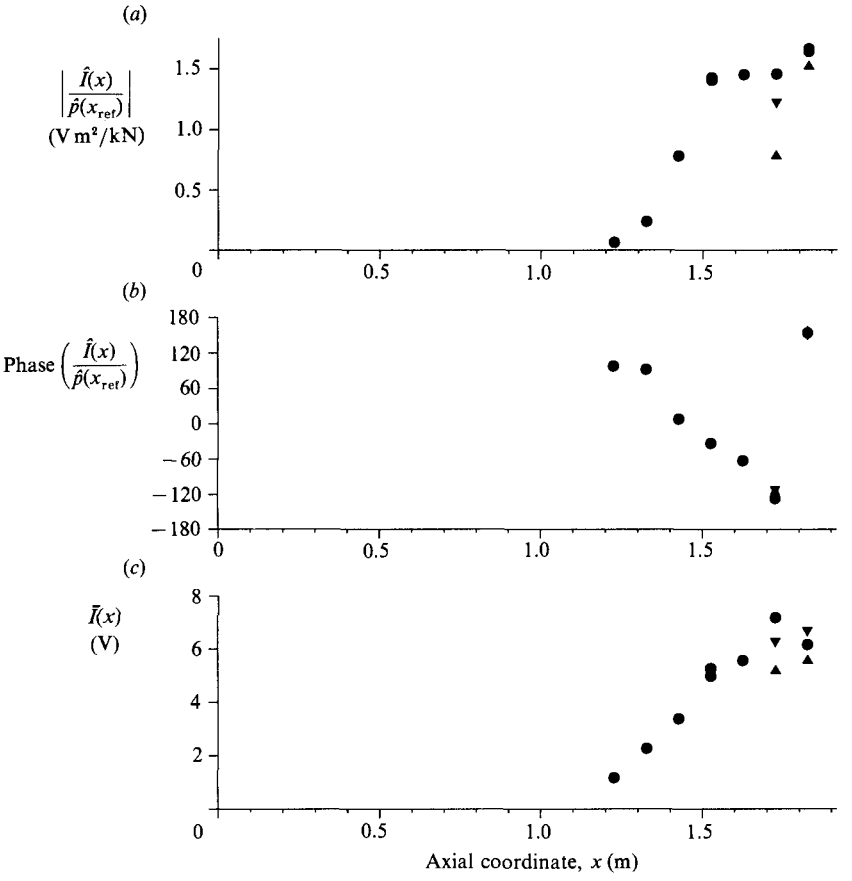

FIGURE 7. The mean and unsteady light emission data for configuration 1, $\phi = 0.57$ and forcing at 45 Hz with an amplitude of centre-body motion of ▲, 3.1 mm; ●, 2.4 mm; ▼, 1.7 mm peak-to-peak.

figure 7*c*). We have already verified that the heat release rate is proportional to light emission and so we can write

$$\bar{q}(x) = \begin{cases} 0 & \text{for} \quad x < x_G, \\ \kappa(x - x_G) & \text{for} \quad x > x_G. \end{cases} \tag{3.1}$$

Integration along the duct shows

$$\bar{m} c_p \Delta T_0 = \int_0^L \bar{q}(x)\,\mathrm{d}x = \tfrac{1}{2}\kappa(L - x_G)^2. \tag{3.2}$$

The constant of proportionality, κ, may therefore be determined from the measured rise in stagnation temperature and was found to be 0.66 MW/m².

The amplitude of the unsteady light emission per unit length is found to be roughly proportional to the mean light emission (compare the shapes of figures 7*a* and *c*). This linear relationship also occurred in the unforced combustion oscillations described in Part 1. The phase of the heat release rate along the duct also has a striking pattern in the forced experiments. At each frequency, the phase of the heat release rate decreases linearly along the duct (see figure 7*b*), indicating an increasing time delay.

Furthermore the negative slope of the phase with respect to axial position steepens linearly with increasing frequency, implying that perturbations in heat release rate propagate down the duct with the same constant velocity for all frequencies. Calculations identify this velocity as the mean velocity at the gutter lip, $\bar{u}_G$. Similar trends were observed in Part 1 for low amplitudes of the unforced combustion oscillation. These observations can be combined into a statement that the fractional change in heat release rate/unit length at an axial position x is equal to the fractional change at the gutter at a time $\tau(x)$ earlier, i.e.

$$\frac{\hat{q}(x)}{\bar{q}(x)} = \frac{\hat{q}_G}{\bar{q}_G} e^{-i\omega\tau(x)}. \tag{3.3}$$

$\bar{q}_G$ and $\hat{q}_G$ denote the mean and fluctuating heat release rate per unit length at the gutter and $\tau(x)$ is the time taken for the disturbance to travel from the gutter to x, i.e.

$$\tau(x) = (x - x_G)/\bar{u}_G. \tag{3.4}$$

Once the perturbations in the heat release rate at the flame-holder are known, (3.3) can be used to determine the unsteady combustion throughout the duct. The flame at the gutter lip would respond to oncoming changes in particle velocity, pressure, density and temperature. But the Mach number of the mean flow is low and so the fractional changes in velocity are much larger than those in pressure, density or temperature. This was evident in the experimental results described in Part 1 where the flame was observed to move intermittently upstream of the flame-holder (indicating velocity perturbations of the order of the mean velocity), while fractional changes in pressure were less than 10%. Since the oncoming flow is isentropic, the percentage changes in density and temperature are of the same order as those in pressure. As the fractional velocity perturbations are so much larger, it is reasonable to assume that they have the greatest influence on the unsteady combustion near the gutter lip, and we write

$$\frac{\hat{q}_G}{\bar{q}_G} = f\left(\frac{\omega 2\pi r_G}{\bar{u}_G}\right)\frac{\hat{u}_G}{\bar{u}_G}, \tag{3.5}$$

where r_G denotes the radius of the gutter. It is impossible to use a hot wire to measure the velocity at the gutter lip directly, because the flame burns back intermittently. Instead we use a combination of our experimental data and the calculation procedure outlined in §2 to determine the variation of the non-dimensional function f with a Strouhal number $\omega 2\pi r_G/\bar{u}_G$.

First we note that we have already shown that it is reasonable to consider the heat release rate to be proportional to the light emission and we have denoted the constant of proportionality by k. Since $\hat{q}(x)$ is heat release rate per unit length and $\hat{I}(x)$ is the light emission in windows of 0.1 m lengths,

$$\hat{q}(x) = 10k\hat{I}(x). \tag{3.6}$$

The mean and fluctuating light emission data have been scaled by $10k$ in figure 8 to convert them into estimates of the heat release rates per unit length.

The calculation procedure described in §2 may be used to determine the relationship between velocity fluctuations at the gutter lip and pressure perturbations at the reference position x_{ref}. The upstream acoustic boundary condition is complicated in these forced experiments. There is a perforated plate with choked holes and a nozzle with an oscillating centre-body. Rather than attempt to calculate

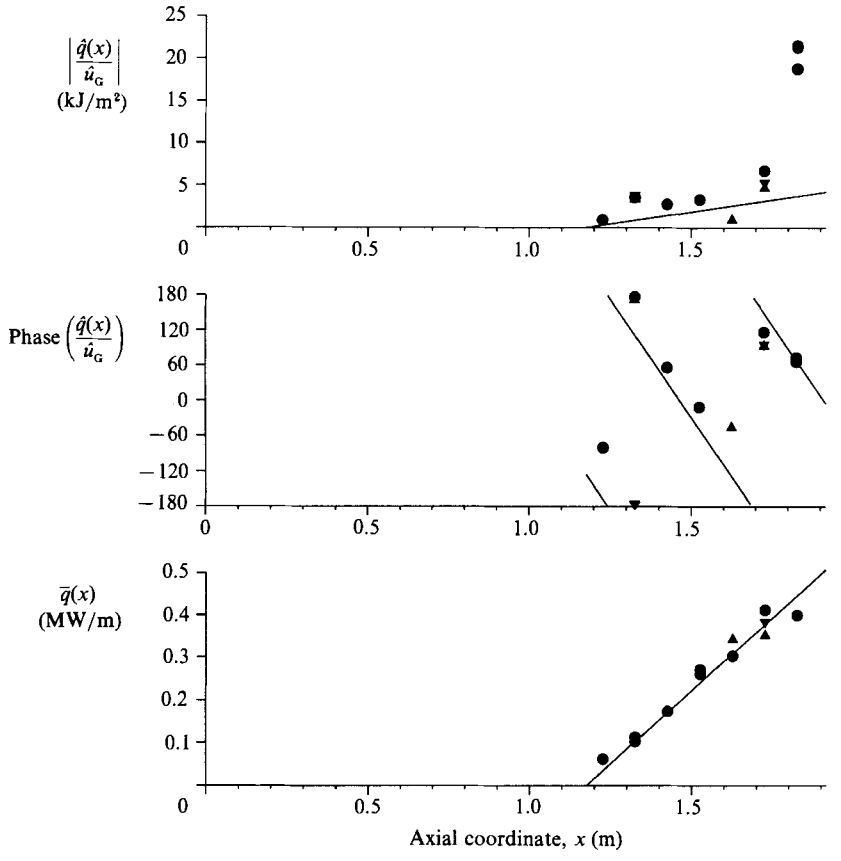

FIGURE 8. The mean and unsteady heat release rates/unit length for configuration 1, $\phi = 0.57$ and forcing at 85 Hz with an amplitude of centre-body motion of ▲, 3.1 mm; ●, 2.4 mm; ▼, 1.7 mm peak-to-peak. ——, weak flame model (defined by (3.1), (3.4) and (3.8)).

the boundary condition this source imposes on the acoustic waves, we have measured the impedance $\hat{p}/\hat{u}$ at the reference position $x_{\text{ref}} = 0.75$ m for each of the forcing frequencies. If in addition we assume the flow to be isentropic upstream of the flame, the flow perturbations are known at x_{ref}. Equation (2.11) may therefore be integrated with respect to x for each forcing frequency ω, and together with the jump condition (2.12) describes the development of the unsteady flow upstream of the flame. A combination of the calculated value of $\hat{p}(x_{\text{ref}})/\hat{u}_G$ with the experimental data for $\hat{I}(x)/\hat{p}(x_{\text{ref}})$ and (3.6) leads to $\hat{q}(x)/\hat{u}_G$. A typical set of results is shown in figure 8.

For each frequency of forcing the phase of $\hat{q}_G/\hat{u}_G$ (which is the phase of f in (3.5)) can be estimated from the measurements by projecting a straight line through the values of $\hat{q}(x)/\hat{u}_G$ back to $x = x_G$, the gutter lip. Such points are plotted in figure 9 as a function of the Strouhal number $St = \omega 2\pi r_G/\bar{u}_G$ and trends begin to emerge. The phase of f varies rapidly at low Strouhal numbers. In this range the phase decreases approximately linearly with Strouhal number as it would if the flame response involved a constant time delay. The phase is π at $St = 0$ and subsequently decreases like $\pi - \beta St$, where the constant β has a value of about $\frac{11}{2}\pi$. At higher Strouhal numbers the phase is almost constant at a value of $-\frac{1}{2}\pi$, the transition

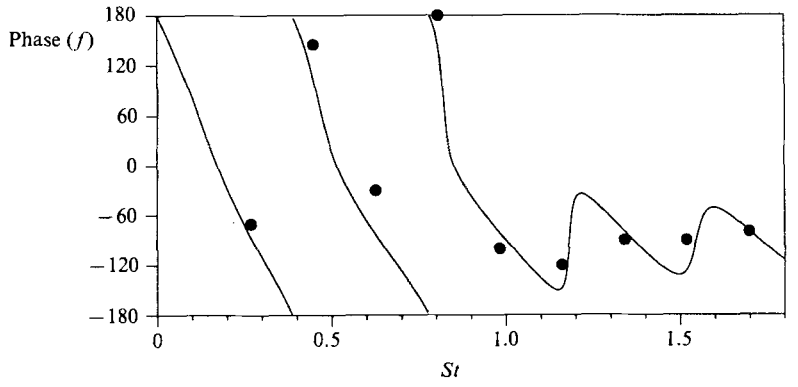

FIGURE 9. The variation of the phase of f (=phase of $(\hat{q}_G/\hat{u}_G)$) with Strouhal number $St = \omega 2\pi r_G/\bar{u}_G$. ●, phase of the extrapolated experimental points; ——, phase of the function f as defined in (3.7).

occurring near $St = 1$. These observations suggest that the phase of f would be adequately represented by a function of the form

$$f(St) = \frac{1}{\mathrm{i}St}\left(1+\frac{\mathrm{e}^{-\mathrm{i}\beta St}}{\mathrm{i}St}\right). \tag{3.7}$$

The phase of f as given by (3.7) is plotted as a solid line in figure 9 for comparison with the extrapolated experimental points. The model describes the observed variation in phase with reasonable accuracy.

We have concentrated on the phase of $\hat{q}$ because, according to Rayleigh's criterion, it is crucial in determining the stability of the flow. However, the function in (3.7) also accounts very roughly for the observed changes in the magnitude of $\hat{q}_G/\hat{u}_G$. In particular it predicts a reduction in the magnitude of f as the Strouhal number increases, which is consistent with the observations.

Collecting together the information in (3.3), (3.5) and (3.7) leads to

$$\frac{\hat{q}(x)}{\bar{q}(x)} = \frac{1}{\mathrm{i}St}\left(1+\frac{\mathrm{e}^{-\mathrm{i}\beta St}}{\mathrm{i}St}\right)\frac{\hat{u}_G}{\bar{u}_G}\,\mathrm{e}^{-\mathrm{i}\omega\tau(x)}, \tag{3.8}$$

an empirical flame model which describes how perturbations in the flow influence the rate of heat release. Velocity fluctuations at the gutter lip perturb the flame in the vicinity of the gutter, the local Strouhal number $St = \omega 2\pi r_G/\bar{u}_G$ determining the susceptibility of the flame to changes in the flow. The rate of heat release at an axial position x, downstream of the flame holder, mimics the change at the gutter lip after a time delay $\tau(x) = (x-x_G)/\bar{u}_G$.

The frequencies of combustion instabilities occurring in this rig measured in Part 1 were found to be in the range 70–120 Hz. The Strouhal number, St, is greater than unity at all these frequencies and (3.8) can be roughly approximated to

$$\frac{\hat{q}(x)}{\bar{q}(x)} = \frac{\hat{u}_G}{\mathrm{i}St\bar{u}_G}\,\mathrm{e}^{-\mathrm{i}\omega\tau(x)}. \tag{3.9}$$

Since $St = \omega 2\pi r_G/\bar{u}_G$ this is equivalent to

$$\frac{\hat{q}(x)}{\bar{q}(x)} = \frac{\hat{\eta}_G}{2\pi r_G}\,\mathrm{e}^{-\mathrm{i}\omega\tau(x)}, \tag{3.10}$$

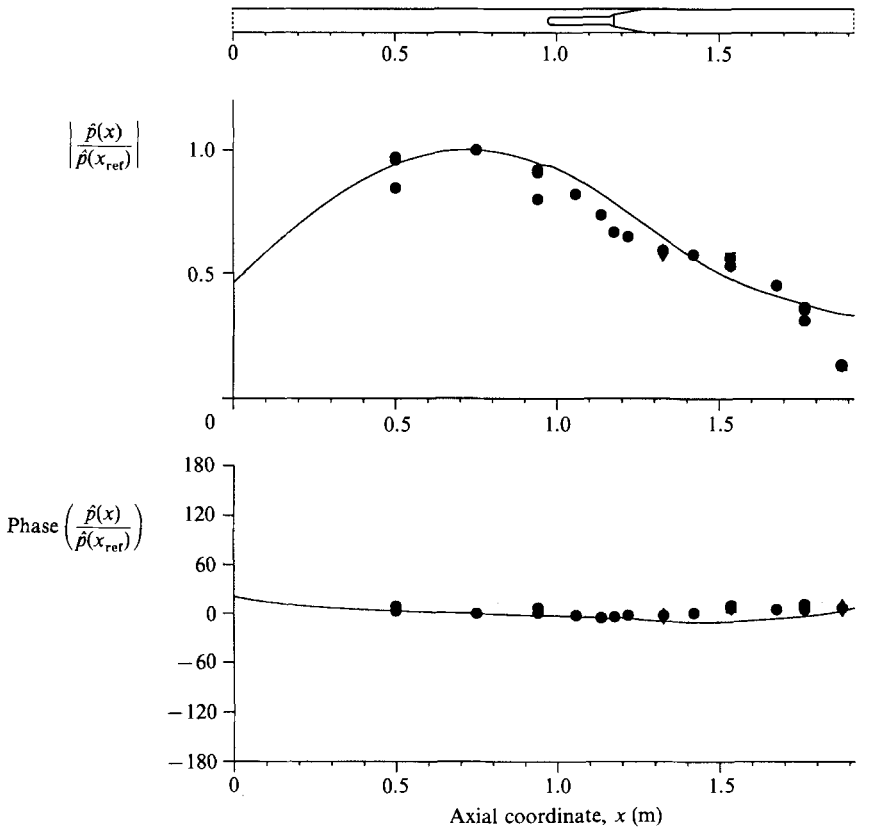

FIGURE 10. The pressure variation along the duct for configuration 1, $\phi = 0.57$ and forcing at 85 Hz with an amplitude of centre-body motion of ▲, 3.1 mm; ●, 2.4 mm; ▼, 1.7 mm peak-to-peak. ——, calculated using the weak flame model.

where η_G is the particle displacement at the gutter lip. The unsteady heat release rate at the gutter lip is evidently in phase with the particle displacement of premixed gas at the gutter, the fractional change in the heat release rate being equal to the amplitude of the perturbation in particle displacement divided by the circumference of the gutter.

Equations (3.1), (3.4) and (3.8) give functional forms for the mean and unsteady heat release rate per unit duct length. These forms are compared with the scaled experimental data in figure 8. The mean heat release rate and the phase of the unsteady heat release rate are well represented by the model. The agreement between the form in (3.8) and experimental results for the magnitude of the unsteady heat release rate is less satisfactory. But the importance of this inaccuracy in the model may be tested by using it in the calculation procedure described in §2.

The unsteady flow at x_{ref} has been measured for each forcing frequency. Equations (2.2) and (2.11) may therefore be integrated throughout the duct with $\bar{q}(x)$ and $\hat{q}(x)$ as specified in (3.1) and (3.8) and, together with the jump conditions across the control volumes, determine the flow throughout the duct for a particular forcing frequency. Figure 10 shows a typical comparison between measured and calculated pressure mode shapes. The theory predicts a mode of roughly the right shape. However, the exit boundary condition is not satisfied exactly, the degree to which

the predicted exit pressure perturbation differs from zero being an indication of the inaccuracy of the flame model.

The ultimate test of the flame model will be how effectively it can predict the frequency and mode shapes for the combustion instabilities which occur at higher equivalence ratios. But the flame model needs some extension before it can be applied at these higher equivalence ratios.

At the low equivalence ratio ($\phi = 0.57$) used in these forced experiments the light emission/unit length increases linearly along the duct as shown in figure 7(c). However, as the equivalence ratio is increased, the distribution of the mean light emission along the duct changes (see Part 1, figure 12*a*). Our ultimate aim is to develop a prediction scheme for afterburners, for which there are existing codes to calculate the axial distribution of the mean heat release rate. So rather than develop a theory to calculate $\bar{q}(x)$ for our rig geometry, we will use an empirical form which describes our observations. Calculation of the unsteady flow is our main objective.

We approximate $\bar{q}(x)$ by three straight lines

$$\bar{q}(x) = \begin{cases} 0 & \text{for} \quad x < x_G, \\ B(\phi)(x-x_G)/(x_R-x_G) & \text{for } x_G < x < x_R, \\ B(\phi)+C(\phi)(x-x_R)/(L-x_R) & \text{for } x_R < x < L, \end{cases} \tag{3.11}$$

x_R is four duct diameters downstream of x_G and is near the end of the recirculation zone (Zukoski 1978). $B(\phi)$ and $B(\phi)+C(\phi)$ are the mean heat release rates per unit length at x_R and the end of the duct, $x = L$, respectively. The ratio $B(\phi)/C(\phi)$ is to be chosen to be consistent with the observed trends in the light emission data. For a low value of equivalence ratio ($\phi = 0.57$), the light emission per unit length increases linearly with the same slope along the whole duct. Hence $B(0.57) = C(0.57)(x_R-x_G)/(L-x_R)$. At an intermediate equivalence ratio ($\phi = 0.63$), the light emission per unit length is constant between x_R and the duct end, i.e. $C(0.63) = 0$. For still higher equivalence ratios the light emission per unit length is found to have a maximum at x_R indicating that $C(\phi)$ is negative. A functional form for the ratio $B(\phi)/C(\phi)$ consistent with these trends has been developed (Bloxsidge 1987), but the real test is how well the simple form for $\bar{q}(x)$ in (3.11) describes the light emission data.

The magnitude of $B(\phi)$ and $C(\phi)$ can be expressed in terms of the combustion efficiency, η, which we take to be a function of equivalence ratio. Integration of (3.11) along the duct shows that

$$\int_0^L \bar{q}(x)\,\mathrm{d}x = \tfrac{1}{2}B(\phi)(x_R-x_G)+\{B(\phi)+\tfrac{1}{2}C(\phi)\}(L-x_R). \tag{3.12}$$

This integral of $\bar{q}(x)$ is the total heat released/unit time within the duct. It is equal to $\bar{m}\eta(\phi)\Delta H(\phi)$, where $\Delta H(\phi)$ is the maximum heat that can be released by burning 1 kg of premixed ethylene and air with an equivalence ratio ϕ; $\Delta H(\phi) = 3.2\phi/(1+0.067\phi)$ MJ/kg for $\phi < 1$. Since $\eta(\phi)\Delta H(\phi)$ is the mean heat released within the duct per unit mass, it is equal to $c_p \Delta T_0$. The rise in stagnation temperature, ΔT_0, has been measured for two equivalence ratios and these measurements give $\eta(0.57) = 0.8$ and $\eta(0.70) = 0.9$. Intermediate combustion efficiencies can be deduced by interpolation.

At low fuel–air ratios the unsteady light emission due to the combustion instabilities studies in Part 1 has a form similar to the forced oscillations investigated in this section. The phase of the light emission decreases linearly with axial distance

x, as appropriate for the convection of disturbances downstream with little change in shape at the mean gutter lip velocity, $\bar{u}_G$. In Part 1 we have called this form of oscillation 'convecting behaviour'. For higher fuel–air ratios, at which the natural oscillations have a higher amplitude, the instantaneous light emission data was found to have a different form in the downstream portion of the duct. There the local light emission is intense over part of a buzz cycle, but nearly zero over the rest, indicating that there is no combustion throughout a significant proportion of the cycle. The initiation of combustion convects down the duct, but the combustion at downstream positions is extinguished before that at points further upstream. The effect of this on the phase of the heat release rate is described in Part 1. For these higher amplitude oscillations the phase of the heat release rate/unit length only decreases linearly with axial distance, like a disturbance convecting with velocity $\bar{u}_G$, for a short axial distance to a position where the local heat release rate and pressure perturbations are in phase. Downstream of this point in the duct, the phase of the heat release is almost constant and calculations showed that an appropriate convection velocity in this region is the sound speed. We have called this mode 'established buzz' and must generalize the form for $\tau(x)$, the time delay between combustion oscillations at x and at the gutter lip to describe the unsteady heat release rate in this mode. For weak disturbances we have from (3.4)

$$\tau(x) = (x - x_G)/\bar{u}_G. \tag{3.13a}$$

For larger amplitude disturbances we will take

$$\tau(x) = \begin{cases} (x - x_G)/\bar{u}_G & \text{for } x < x_0, \\ (x_0 - x_G)/\bar{u}_G + \int_{x_0}^{x} \mathrm{d}x/\bar{c}(x) & \text{for } x > x_0, \end{cases} \tag{3.13b}$$

where x_0 is the axial position at which $\hat{p}(x)$ and $\hat{q}(x)$ are first in phase downstream of the gutter lip. We will refer to the prescription of the heat release rate defined by (3.8), (3.11) and (3.13a) as the 'weak flame model' because it is appropriate for weak buzz. At higher levels of the oscillation the appropriate form of heat release is described by (3.8), (3.11) and (3.13b). We will denote this as the 'established flame model'.

In summary then, the axial variation of the mean heat release rate has been approximated by three straight lines as shown in (3.11). The functions $B(\phi)$ and $C(\phi)$ are chosen to fit experimental data.

Experimental data has been used to describe the response of a flame to perturbations at the flame holder and a model of the distributions of unsteady heat release rate has been developed. The result is displayed in (3.8). The unsteady heat release rate at the gutter lip is related to the local velocity perturbation in a way that depends on the Strouhal number $St = \omega 2\pi r_G/\bar{u}_G$. The fluctuation in heat release rate at an axial position x, downstream of the flame-holder mimics the change at the gutter lip after a time delay $\tau(x)$. This time delay has two distinct forms, depending on the amplitude of the disturbances. For low levels $\tau(x) = (x - x_G)/\bar{u}_G$, while for higher amplitudes the time delay is far less (see (3.13)). Since our theory is linear it cannot distinguish which is the appropriate form. Therefore we will have two predicted frequencies and mode shapes for each geometry. Comparison with experiment will indicate which is the required form.

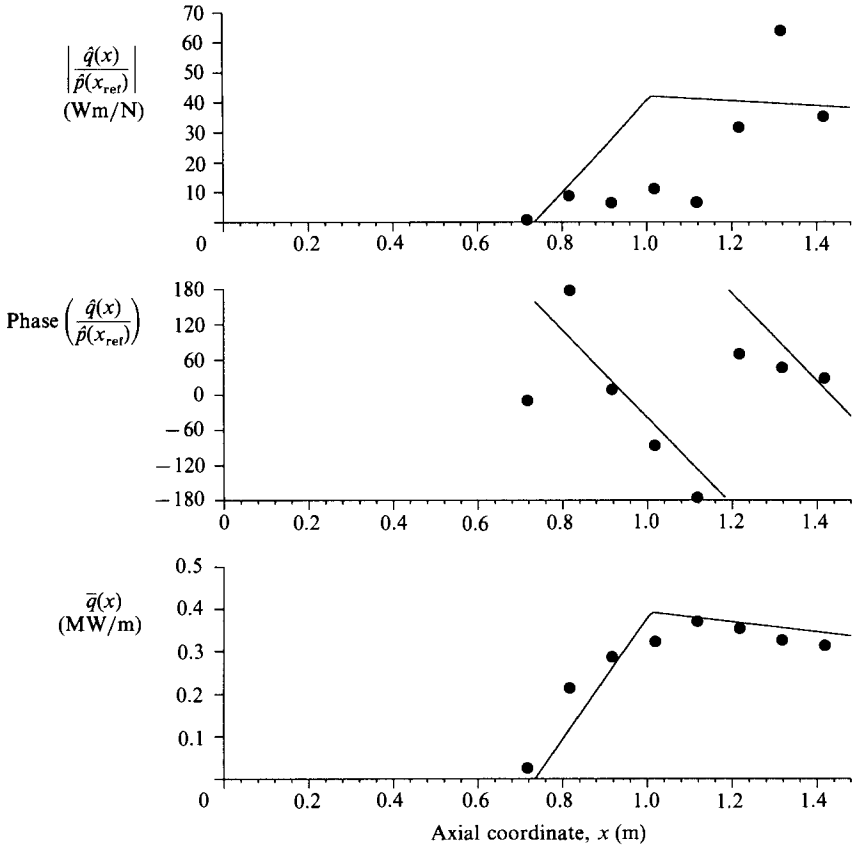

FIGURE 11. The mean and unsteady heat release rates/unit length at the buzz frequency for configuration 2, $\phi = 0.65$. ●, experimental points; ——, weak flame model.

4. Comparison of theory and experiment

A stable flame has been excited at a number of discrete frequencies to determine the relationship between changes in heat release rate and flow perturbations. The idea behind such an investigation is that the response of the flame to perturbations at the flame-holder would have a universal form that could be applied in different geometries and flow conditions. We now test that hypothesis by seeing whether the same flame model is consistent with the observations of combustion instabilities reported in Part 1. We will compare the form for the axial distribution of the heat release rate in (3.8), (3.11) and (3.13) with measured light emission data for a range of duct lengths, gutter positions and running conditions. The combustion oscillations were investigated for the geometry illustrated in figure 1, with a fixed choked nozzle at the inlet to the working section and an open end downstream. The theory described in §2 and the flame model developed in §3 enable the mean and fluctuating flow to be calculated. An iteration in the complex-valued frequency to satisfy the boundary conditions determines the eigenfrequencies. A comparison will be made between the predicted and measured frequencies and the pressure mode shape. In addition, the amplitudes of linear disturbances are proportional to $\exp(-\operatorname{Im}\omega t)$. When $\operatorname{Im}\omega$ is negative, linear disturbances grow exponentially until limited by

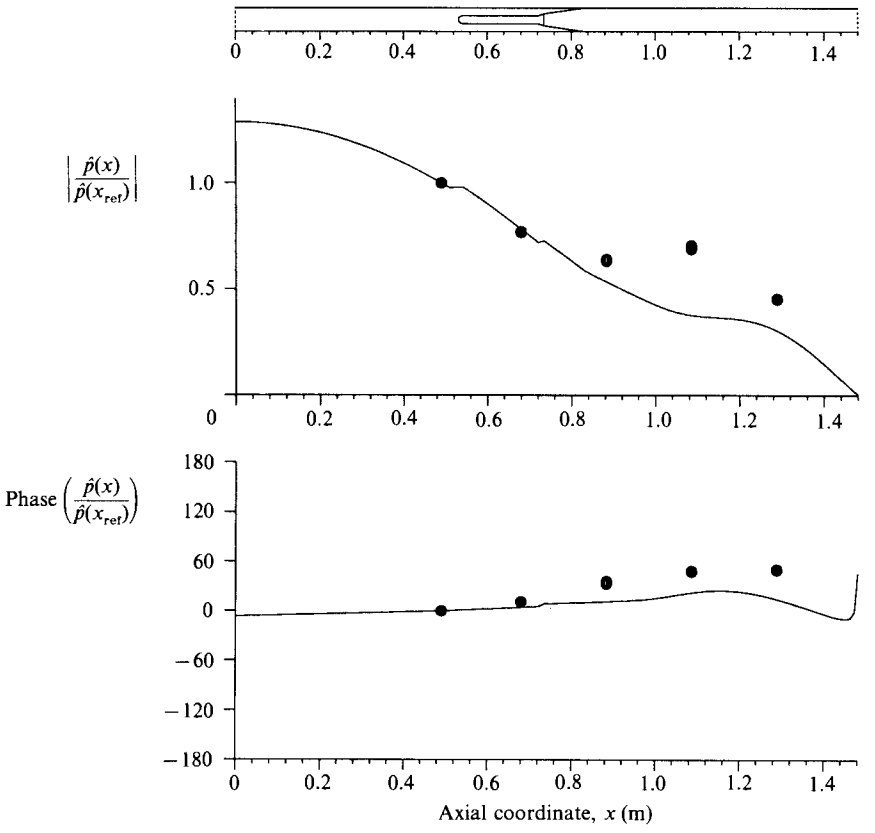

FIGURE 12. The pressure variation along the duct at the buzz frequency for configuration 2, $\phi = 0.65$. ●, experimental points; ——, calculated using the weak flame model.

nonlinear effects. Since $-\operatorname{Im}\omega$ describes the rate of growth of linear disturbances, it is a measure of the driving to instability.

As a first test we will apply the theory of configuration 1 at an equivalence ratio of 0.70. This case was considered in §2 where the local heat release rates were estimated by a least-square cubic-spline fit to the light emission data (see figure 3). There the calculated frequency was 76.4 Hz in excellent agreement with the measured value of 77 Hz, and the growth rate was found to be $+47\ s^{-1}$. The dotted lines in figure 3 show the comparison between the established flame model in (3.8), (3.11) and (3.13*b*) and the measured light emission data. While these analytical forms do not, of course, fit the data quite as accurately as the least-squares approximation, the main trends are still well represented. When this flame model was used in the calculation procedure, the frequency of the combustion instability was found to be 81.7 Hz and the growth rate $+1.1\ s^{-1}$. This gives an indication of the error induced by a less accurate representation of the local heat release rates. The growth rate is somewhat less than for the spline fit to the heat release rates. However, the frequency is well predicted. The dotted lines in figure 4 show the calculated pressure mode shapes. It is evident from this diagram that the jump conditions across the two abrupt contractions in area and the control volume downstream of the gutter (as described by (2.12) and (2.15)–(2.17)) actually have very little effect. There is reasonable agreement between the calculated and measured pressure mode shapes.

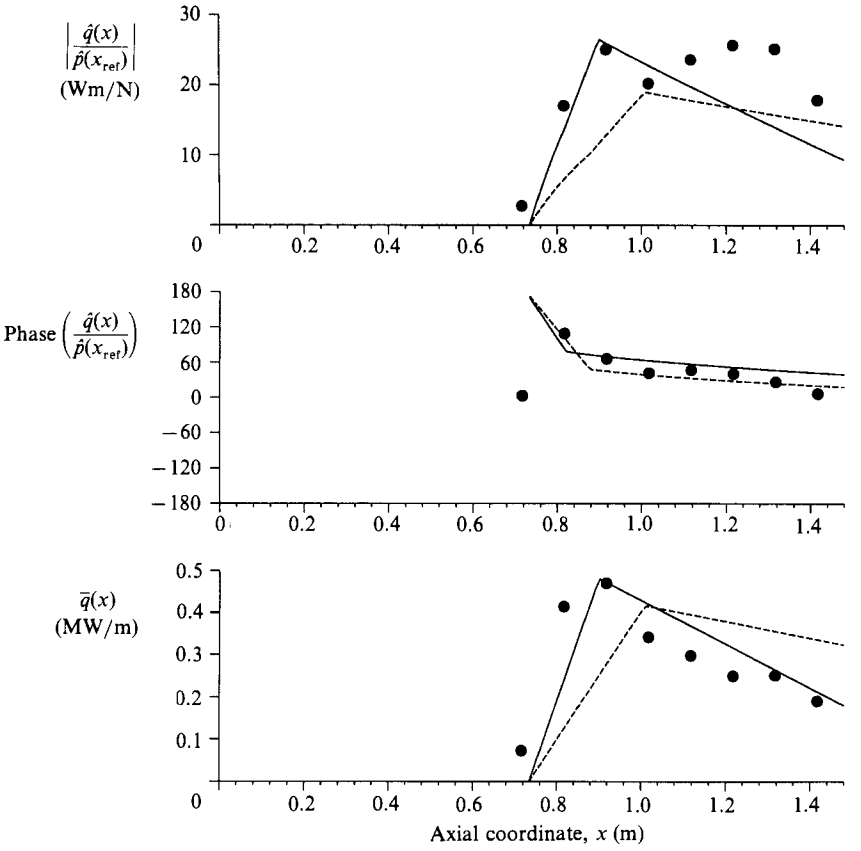

FIGURE 13. The mean and unsteady heat release rates/unit length at the buzz frequency for configuration 2, $\phi = 0.66$. ●, experimental points; – – –, established flame model; ——, established flame model with improved description of the mean heat release rate.

Configuration 2 has a shorter length between the inlet to the working section and the gutter lip than configuration 1, but the same burning length between the gutter and duct exit. The combustion instabilities in configuration 2 have been investigated extensively for a range of fuel–air ratios. Representative experimental results are reported in Part 1. It was found that when the equivalence ratio is less than 0.66 fluctuations in heat release rate convect with the gutter lip velocity $\bar{u}_G$ along most of the duct, while for $\phi > 0.66$ the information travels more rapidly.

Figure 11 shows a comparison of the measured light emission data for $\phi = 0.65$, scaled by k to convert it into heat release rates/unit length, with the weak flame model in (3.8), (3.11) and (3.13a). The flame model gives an excellent prediction for the mean heat release rate and the phase of the fluctuations. Once again the amplitude of the unsteady heat release is less accurately represented. The calculated frequency was found to be 75.5 Hz in comparison with the measured value of 81 Hz. The growth rate of $-4.4\ s^{-1}$ indicates that the flame is predicted to be just stable and the oscillations were everywhere found to be of low amplitude. Figure 12 shows the measured and predicted pressure mode shapes.

For equivalence ratios above 0.66, the phase of the unsteady heat release rate is given by (3.13b). The flame model of §3 is compared with light emission data for

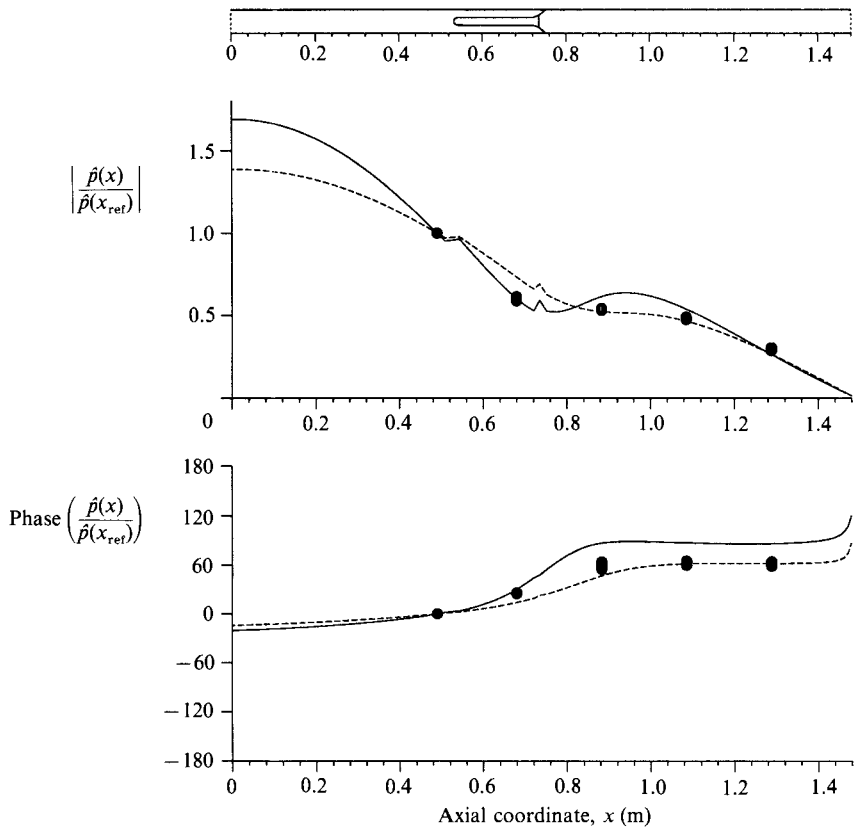

FIGURE 14. The pressure variation along the duct at the buzz frequency for configuration 2, $\phi = 0.66$. ●, experimental points; – – –, calculated using the established flame model; ——, calculated using the improved description of the mean heat release rate shown in figure 13.

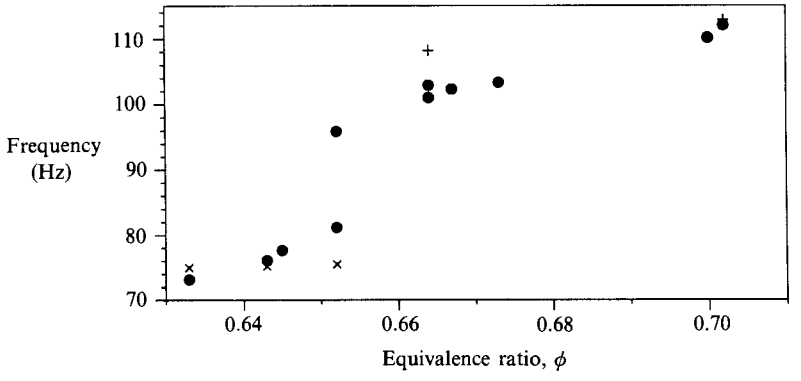

FIGURE 15. The variation of the frequency of the combustion oscillation with equivalence ratio for configuration 2. ●, experimental points; ×, calculated using the weak flame model; +, calculated using the established flame model with an improved description of the mean heat release rate.

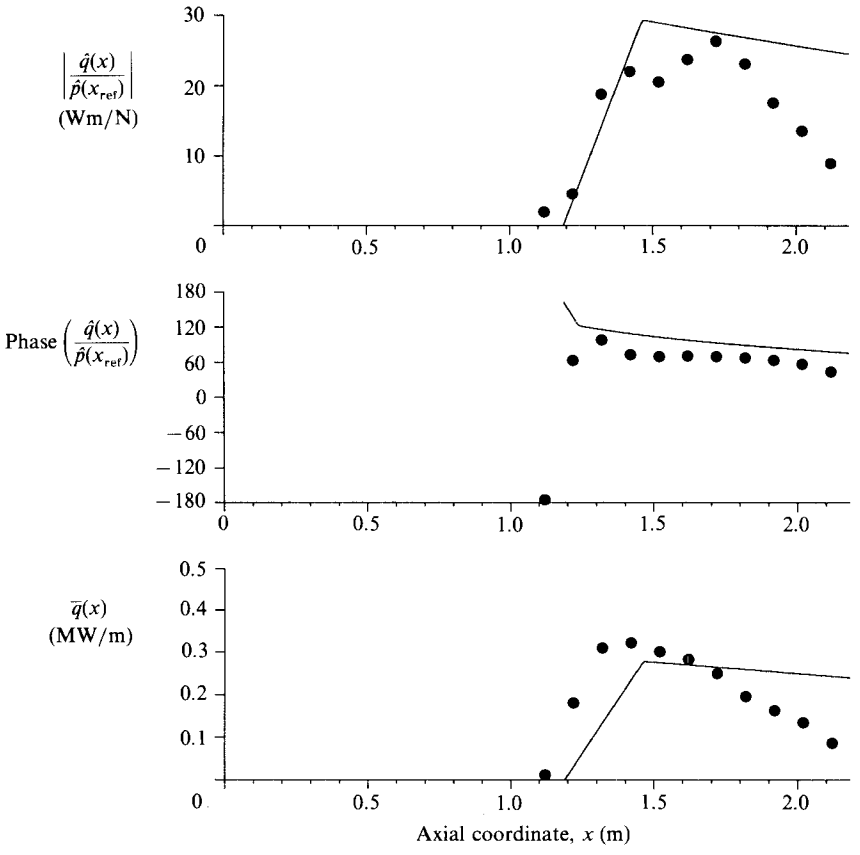

FIGURE 16. The mean and unsteady heat release rates/unit length at the buzz frequency for configuration 3, $\phi = 0.65$. ●, experimental points; ——, established flame model.

$\phi = 0.66$ in figure 13. Two different piecewise linear approximations to the mean heat release rates are presented. These enable us to investigate the importance of a correct estimate of the distribution of mean heat release rate in a calculation of the unsteady flow. The description of the mean heat release rate in (3.8) leads to the form represented by dotted curves in figure 13 and a frequency of the combustion oscillation of 88.3 Hz, differing by 15 Hz from the measured value of 103 Hz. It is clear from figure 13 that in this form for the mean heat release rate x_R, the position of the maximum in the heat release rate/unit length, has been taken too far downstream and the heat release rate close to the gutter underestimated. When the description of the mean heat release rate is improved to the form indicated by solid lines in figure 13 by taking $x_R = x_G + 0.16$ m and $B/C = -1.6$, calculations with the flame model in (3.11) and (3.13*b*) give a frequency of 108 Hz, in much better agreement with the observations. The growth rate is calculated to be $+79\ s^{-1}$. The theoretical and measured pressure mode shapes are compared in figure 14. The theory is accurately able to predict the pressure variation along the duct.

We have seen that the theory reproduces the observed rapid rise in frequency as the form of the oscillation changes from weak to established buzz. Figure 15 shows the variation of the predicted and measured frequencies with equivalence ratio for this transition. The growth rate was also found to increase considerably at the

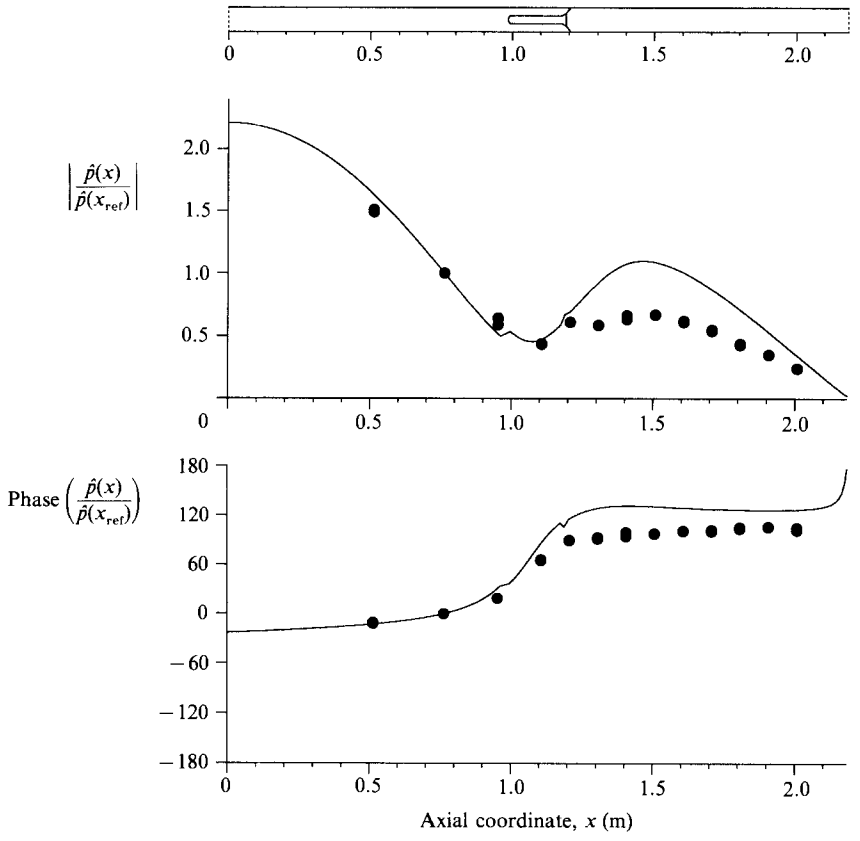

FIGURE 17. The pressure variation along the duct at the buzz frequency for configuration 3, $\phi = 0.65$. ●, experimental points; ——, calculated using the established flame model.

transition from weak to established buzz, from a value of $-4.4\ s^{-1}$ at $\phi = 0.65$ to $+79\ s^{-1}$ at $\phi = 0.66$. This indicates a dramatic increase in the driving to instability. In the experiment a corresponding rise in the amplitudes of the oscillations was observed.

Figures 16 and 17 show a comparison of theory and experiment for configuration 3 in which the burning length is extended. The calculated frequency was found to be 80.1 Hz, again in good agreement with the measured value of 77 Hz. The growth rate was $+33\ s^{-1}$, consistent with a large amplitude of instability.

The effect of increasing the flow velocity is shown in figures 18 and 19. Once again the flame model developed in §3 describes the mean and unsteady heat release rates/unit length with reasonable accuracy. The theory correctly predicts the pressure mode shape, and the calculated frequency of 113 Hz is close to the measured value of 109 Hz. It is interesting to note that while some of the pressure data may appear to have a node somewhere near the gutter lip, this is clearly not true in this case with a higher flow rate. This indicates that the simplified acoustic model used by Heitor, Taylor & Whitelaw (1984), in which the pressure is assumed to have a node at the gutter, would be inappropriate here. A more complete analysis of the sort described in this paper is needed to account for the observed changes in mode shape and frequency as the mean flow varies.

These test cases indicate that our theory is well able to predict the frequencies and

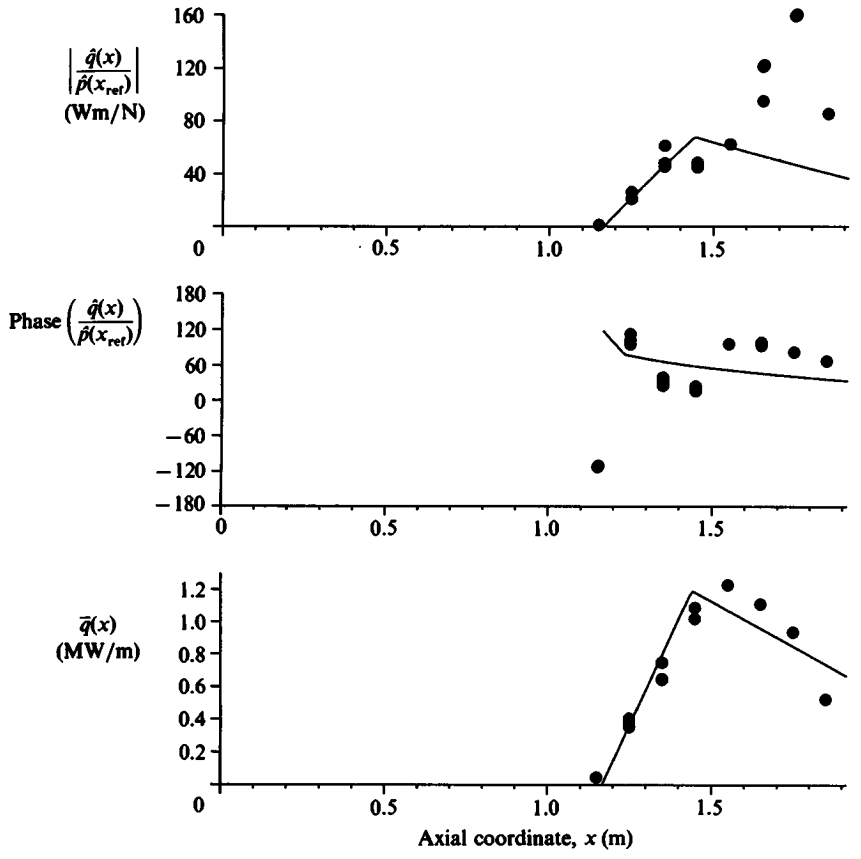

FIGURE 18. The mean and unsteady heat release rates/unit length at the buzz frequency for configuration 4, $\phi = 0.71$. ●, experimental points; ——, established flame model.

mode shapes of the combustion instabilities for different geometries and flow conditions. Figure 20 illustrates theoretical predictions for the effects of changes in inlet Mach number, inlet temperature, upstream length and burning length on the frequency of the instability. Each of these parameters was varied independently from the basic flow and geometry of configuration 2 with $\phi = 0.66$. This is the geometry investigated at various equivalence ratios in figure 15. The frequencies calculated using the weak and established flame models are plotted in the figure. It is interesting to note that the two forms for the unsteady heat release rate lead to very different frequencies, even though the mean flow is the same in both cases. This emphasizes the influence of the unsteady heat release on the frequency and, in particular, throws doubt on some previous calculation schemes where the effect of unsteadiness in the heat release rate on frequency is neglected.

Figure 20(*a*) illustrates that increases in inlet Mach number tend to increase the frequency, consistent with the trend observed on our rig. The growth rate was also found to increase with increasing inlet Mach number, indicating that linear disturbances in the duct/flame arrangement grow more rapidly.

The second parameter to be varied was the inlet static temperature $\bar{T}_u$. For both weak and established buzz, the frequency increases (see figure 20*b*) and in fact the growth rate decreases with increasing inlet temperature. The increase in frequency

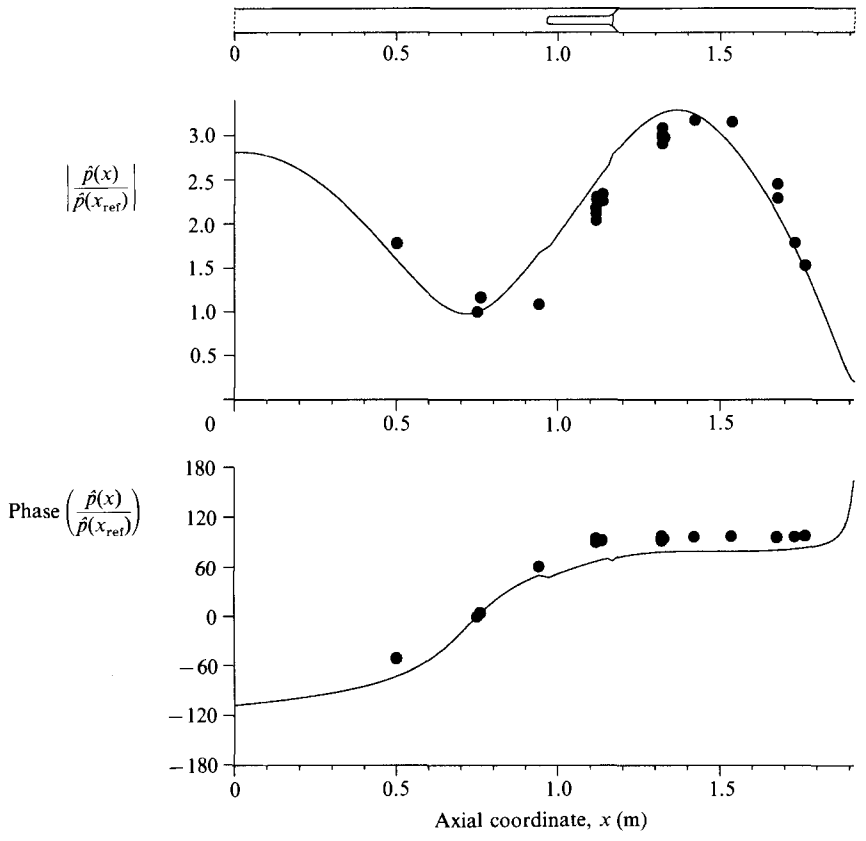

FIGURE 19. The pressure variation along the duct at the buzz frequency for configuration 4, $\phi = 0.71$. ●, experimental points; ——, calculated using the established flame model.

can be explained by the fact that travel times are reduced since both the sound speed and the convection velocity increase like $\bar{T}^{\frac{1}{2}}$. The prediction that the growth rate decreases as the inlet temperature is increased is consistent with expectations that the rig should be more stable with a preheated inlet flow.

Finally, the effect of geometry changes are investigated in figure 20 (c, d). As might have been expected, an increase in either the upstream length, x_{G}, or in the burning length $L - x_{\text{G}}$, decreases the frequency of the oscillation.

5. Conclusions

A series of experiments have been undertaken to investigate the response of a confined premixed flame to excitation. The general trends observed in these experiments have been used to derive an empirical flame model which describes the relationship between the unsteady heat release rate/unit length and flow perturbations at the flame holder. Two different types of buzz occur, denoted by weak and established buzz. They are associated with low- and higher-amplitude oscillations respectively. The model describes both forms with reasonable accuracy, but cannot predict the transition between them.

This flame model has been used in the one-dimensional conservation equations of mass, momentum and energy to determine the frequency and mode shape of the

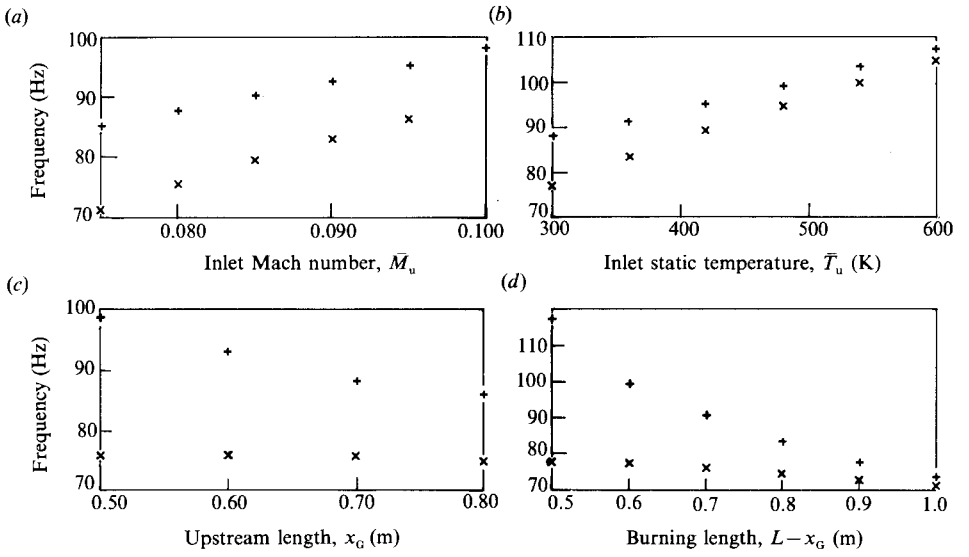

FIGURE 20. The effect of changes in (*a*) inlet Mach number, (*b*) inlet static temperature, (*c*) upstream length and (*d*) burning length on the buzz frequency. The changes are made to a configuration with $\phi = 0.66$, $\bar{M}_u = 0.08$, $x_G = 0.74$ m and $L = 1.48$ m. ×, calculated using the weak flame model; +, calculated using the established flame model.

oscillation. The theory has been checked by comparison with the experimental results of Part 1. The results are encouraging. Calculated and measured frequencies lie within 6 Hz of each other, indicating a maximum error of 7%. In addition, the theory is able to predict the observed trends in variations in frequency as equivalence ratio, inlet Mach number or duct geometry are changed.

This work was funded by Rolls-Royce plc and carried out at the University of Cambridge Engineering Department while one of the authors (G.J.B.) was in receipt of an SERC studentship.

REFERENCES

BARTON, J. P. 1986 Acoustic and entropy wave input–output relationships for quasi-one-dimensional gas flows. *J. Acoust. Soc. Am.* **80**, 340–346.

BLOXSIDGE, G. J. 1987 Reheat buzz – an acoustically driven combustion instability. Ph.D. thesis, University of Cambridge.

BLOXSIDGE, G. J., DOWLING, A. P., HOOPER, N. & LANGHORNE, P. J. 1988 Active control of reheat buzz. *AIAA J.* (to appear).

BRAY, K. N. C., CAMPBELL, I. G., LEE, O. K. L. & MOSS, J. B. 1983 An investigation of reheat buzz instabilities. *Dept Aeronautics and Astronautics, Southampton University, Rep.* AASU 83/2.

CAMPBELL, I. G., BRAY, K. N. C. & MOSS, J. B. 1983 Combustion oscillations in a ducted premixed flame. *Combustion in Engineering*, IMechE, pp. 85–94.

CUMPSTY, N. A. 1979 Jet engine combustion noise: pressure, entropy and vorticity perturbations produced by unsteady combustion or heat addition. *J. Sound Vib.* **66**, 527–544.

DOWLING, A. P. & BLOXSIDGE, G. J. 1984 Reheat buzz – an acoustically driven combustion instability. *AIAA*-84-2321.

HADVIG, S. 1971 Combustion instability: system analysis. *J. Instit. Fuel* **44**, 550–558.

HEITOR, M. V., TAYLOR, A. M. K. P. & WHITELAW, J. H. 1984 Influence of confinement on combustion instabilities of premixed flames stabilized on axisymmetric baffles. *Combust. Flame* **57**, 109–121.

HOWE, M. S. 1979 Attenuation of sound in a low Mach number nozzle flow. *J. Fluid Mech.* **91**, 209–229.

LANGHORNE, P. J. 1988 Reheat buzz: An acoustically coupled combustion instability. Part 1. Experiment. *J. Fluid Mech.* **193**, 417–443.

LE CHATELIER, C. & CANDEL, S. M. 1981 Flame spreading in compressible duct flow. *Proc. First Intl Specialists Meeting of the Combustion Institute, Bordeaux*, pp. 236–242.

MARBLE, F. E. & CANDEL, S. M. 1978 An analytical study of the non-steady behaviour of large combustors. *Proc. 17th Symp. (Intl) on Combustion, The Combustion Institute*, pp. 761–769.

MERK, H. J. 1956 Analysis of heat-driven oscillations. *Appl. Sci. Res.* A **7**, 175–191.

MUGRIDGE, B. D. 1980 Combustion driven oscillations. *J. Sound Vib.* **70**, 437–452.

POINSOT, T., LE CHATELIER, C., CANDEL, S. M. & ESPOSITO, E. 1986 Experimental determination of the reflection coefficient of a premixed flame in a duct. *J. Sound Vib.* **107**, 265–278.

RAYLEIGH, J. W. S. 1896 *The Theory of Sound*. Macmillan.

SUBBAIAH, M. V. 1983 Non-steady flame spreading in two-dimensional ducts. *AIAA J.* **21**, 1557–1564.

ZUKOSKI, E. E. 1978 Afterburners. In *The Aerothermodynamics of Gas Turbine Engines* (ed. G. C. Oates), AFAPL-TR-78-52.